FULafia Journal of Science & Technology
ISSN (print) 2449-0954 \ ISSN (online) 2636-4972
https://lafiascijournals.org.ng/index.php/fjst
Manuscript => **Received:** June, 2026; **Accepted:** Nov., 2026; **Published:** March, 2027 https://doi.org/10.62050/fjst2027.v11n1.880

DYNAMIC ANALYSIS AND QUANTITATIVE FAULT CHARACTERISATION OF A THREE-PHASE INDUCTION MOTOR USING d-q TRANSFORMATION AND MATLAB/Simulink

Ayodeji Joseph Akinremi[1]*, Ignatius Kema Okakwu[1], Ayodeji Akinsoji Okubanjo[1], Ayobami Taiwo Olusesi[2] and Ayo Isaac Oyedeji[2]
[1]Department of Electrical and Electronics Engineering, Olabisi Onabanjo University,
Ago-Iwoye, Ogun State, Nigeria
[2]Department of Computer Engineering, Olabisi Onabanjo University,
Ago-Iwoye, Ogun State, Nigeria
*Corresponding email: akinremi.ayodeji@oouagoiwoye.edu.ng

ABSTRACT
Three-phase induction motors are widely used in industrial drive systems, where electrical faults can produce significant disturbances in current, electromagnetic torque, and rotor speed. This study presents dynamic modelling and quantitative fault characterisation of a three-phase induction motor using the d-q transformation and MATLAB/Simulink. The developed model was used to investigate the motor under no-fault, three-phase symmetrical fault, and unsymmetrical line-to-ground (L-G), line-to-line (L-L), and double line-to-ground (L-L-G) fault conditions. The dynamic responses were evaluated using peak stator current, RMS stator current, minimum rotor speed, percentage speed reduction, minimum electromagnetic torque, peak-to-peak torque variation, and phase current imbalance. Under the no-fault condition, the motor attained a steady-state speed of approximately 1800 rpm. The three-phase fault resulted in a small speed reduction to approximately 1734.14 rpm and a minimum electromagnetic torque of −71.71 Nm. The L- G fault produced a comparatively smaller speed reduction to approximately 1764.10 rpm, although significant current and torque disturbances were observed. The L-L fault produced the highest peak stator current of approximately 226.62 A and the largest peak-to-peak torque variation of 319.49 Nm, while the L-L-G fault produced the phase current imbalance of 70.69%. The results demonstrate that fault severity is dependent on the performance metric considered and that no single dynamic variable is sufficient to comprehensively characterise induction-motor fault behaviour. The proposed quantitative fault characterisation provides useful complementary dynamic indicators for quantitative comparison of induction motor fault responses and provides a simulation-based foundation for subsequent condition monitoring and fault classification studies.

Keywords: d-q transformation, fault analysis, Three-phase induction motor, MATLAB/Simulink, Fault characterisations

INTRODUCTION
Three-phase induction motors are among the most widely used electrical machines in industrial drive and energy conversion systems because of their rugged construction, relatively simple structure, reliability, and suitability for a wide range of applications. Their extensive use in industrial drives has made the reliable operation and condition monitoring of induction motors important considerations in maintaining production continuity and reducing unplanned downtime. Induction motors are, however, susceptible to electrical and mechanical faults that can alter their electromagnetic and mechanical behaviour and eventually lead to equipment failure if the underlying abnormalities are not detected and appropriately addressed (Gangsar & Tiwari, 2020; Hamani *et al.*, 2025). Consequently, understanding the dynamic response of induction motors under healthy and faulty operating conditions is important for the development of effective protection, monitoring, and maintenance strategies.

The dynamic performance of an induction motor is determined by the interaction between its electrical and mechanical subsystems. The stator voltages and currents produce the electromagnetic field, while the resulting electromagnetic torque causes the acceleration and mechanical motion of the rotor. Changes in electrical parameters can therefore affect the mechanical response of the machine, resulting in variations in stator current, electromagnetic torque, rotor speed, and other electromechanical variables. The structure of these dynamics makes transient analysis mainly significant when examining fault conditions. Recent research on induction motor dynamics has highlighted the significance of mathematical models that represent the interaction between electrical and mechanical parameters and replicate transient and steady-state operation. (Konuhova, 2025; Zhou *et al.*, 2024).
Reference-frame transformations offer a conventional method for simplified mathematical representation of electrical machines. The direct–quadrature (d-q)

transformation converts the three-phase variables into orthogonal components, simplifying the phase domain representation while retaining the main electromagnetic and mechanical dynamics of the machine. Therefore, the formulation has been widely utilized in induction motor modelling, transient analysis, control, and fault studies (AL hajzber *et al*., 2021; Sengamalai *et al*., 2022a). Reviews of induction machine fault modelling have also identified d-q models as an important analytical model because they require low computational effort compared with other methods such as finite-element modelling (Terron-Santiago *et al*., 2021).

The availability of numerical simulation environments has further facilitated the investigation of induction motor dynamic behaviour. MATLAB/Simulink provides a suitable environment for implementing nonlinear mathematical models and examining motor responses under different operating conditions. Simulation based studies have demonstrated the application of MATLAB/Simulink for evaluating induction motor performance, dynamic characteristics, and drive behaviour (Konuhova, 2025; Makinde *et al*., 2023). In addition, the use of reduced order and computationally efficient models has been investigated to facilitate the simulation of faulty induction machines while retaining the dynamic information required for fault analysis and condition monitoring (Sapena-Bano *et al*., 2021).

Electrical faults constitute an important category of induction motor abnormalities because they can produce rapid changes in current, torque, and speed. Fault conditions can be broadly distinguished into symmetrical and unsymmetrical disturbances. A three-phase short-circuit fault is symmetrical because the three phases are subjected to essentially similar fault conditions, whereas line-to-ground (L–G), line-to-line (L–L), and double line-to-ground (L–L–G) faults produce phase asymmetry and unequal current distributions. Stator faults can result in characteristic changes in measurable electrical quantities and may produce significant electromagnetic and thermal stresses in the machine (Hussain, 2021; Maraaba *et al*., 2018). Recent investigations have also considered phase related faults using analytical, intelligent, and model based approaches, demonstrating the continuing importance of fault characterisation in induction motor condition monitoring (Dawood *et al*., 2024; Reyes-Malanche *et al*., 2024).

A variety of approaches have consequently been developed for induction motor fault detection and diagnosis. Signal based methods use features extracted from quantities such as stator current, vibration, acoustic signals, or other measurable responses, while model based methods employ mathematical representations of the machine to reproduce and interpret fault induced behaviour. More recently, artificial intelligence and machine learning techniques have been increasingly investigated for automatic fault identification and classification (Bahgat *et al*., 2024; Gangsar & Tiwari, 2020; Hamani *et al*., 2025). Although these approaches can provide effective fault classification, the development of reliable diagnostic techniques requires an understanding of the physical dynamic signatures produced by different fault conditions. Mathematical modelling and simulation therefore remain useful for establishing relationships between fault type and the resulting electrical, mechanical, and electromechanical responses before more advanced diagnostic methods are developed.

Previous simulation-based investigations have demonstrated the usefulness of d-q modelling and MATLAB/Simulink for examining induction motor behaviour under fault conditions. For example, Sebastiaan *et al.* (Sebastian *et al*., 2024) investigated the dynamic responses of a three-phase induction motor under symmetrical and unsymmetrical faults using MATLAB/Simulink, with emphasis on rotor speed, electromagnetic torque, and stator current. Similarly, fault modelling studies have demonstrated that analytical models can reproduce characteristic changes in motor variables under different fault conditions (Terron-Santiago *et al*., 2021). More recent work has continued to investigate fault modelling, diagnosis, and condition monitoring using increasingly sophisticated analytical and data driven techniques (Hamani *et al*., 2025).

Despite these developments, there remains a need for a systematic quantitative comparison of the coupled electrical, mechanical, and electromechanical responses produced by different terminal fault conditions under identical modelling and simulation conditions. Existing simulation studies frequently emphasise waveform observation or selected response variables, which can make it difficult to establish how different faults compare across several dimensions of motor performance. A fault that causes a small rotor speed reduction, for example, may concurrently cause significant RMS current or phase current imbalance, while another fault may produce a much larger torque variation or peak current. Consequently, visual inspection of individual waveforms or reliance on a single performance variable may not provide a sufficiently comprehensive basis for distinguishing the dynamic characteristics of different fault types. This motivates the use of complementary quantitative indicators covering electrical loading, mechanical speed response, electromagnetic torque disturbance, and phase current asymmetry.

Accordingly, this study develops and implements a stationary reference frame mathematical model of a three-phase induction motor in MATLAB/Simulink to investigate and quantitatively compare its dynamic response under normal and electrical fault conditions. Five cases are considered: no-fault operation, a three-phase symmetrical fault, and three unsymmetrical faults comprising L–G, L–L, and L–L–G faults. Each fault is applied at the motor terminal at 1.5 s and cleared after 0.5 s, giving distinct pre-fault, fault, and post-fault intervals within the 3-s simulation. The motor response is evaluated using stator current, electromagnetic torque, and rotor speed, while peak stator current, RMS stator current, minimum rotor speed, percentage speed reduction, minimum electromagnetic torque, peak-to-peak torque variation, and phase current imbalance are employed as quantitative fault signature metrics. This approach extends the conventional waveform-based

analysis by providing measurable indicators through which the electrical, mechanical, and electromechanical effects of the investigated faults can be compared.

The principal contribution of the study is therefore the multidimensional quantitative characterisation of induction motor fault signatures using a common d-q modelling and simulation framework. Rather than assigning fault severity using a single response variable, the study evaluates the different combinations of current stress, phase current asymmetry, speed degradation, and electromagnetic torque disturbance produced by each fault. The results demonstrate that fault severity is metric dependent: the L–L fault produces the highest peak stator current and largest peak-to-peak torque variation, whereas the L–L–G fault produces the highest phase current imbalance and a substantial RMS current response. The L–G fault produces the smallest rotor speed reduction but remains associated with significant electrical and torque disturbances, while the three-phase fault produces pronounced torque disturbance and measurable changes in current and rotor speed. These findings demonstrate that a combination of complementary dynamic indicators provides a more informative representation of induction motor faults than a single performance variable and provides a quantitative foundation for subsequent model-based protection, condition monitoring, and automated fault-classification studies.

The remainder of this paper is organised as follows. Section 2 presents the mathematical formulation of the induction motor using the stationary reference frame and describes the performance metrics used for quantitative fault assessment. Section 3 presents the simulation model, motor parameters, fault configurations, and simulation conditions. Section 4 presents and discusses the dynamic responses and quantitative comparison of the no-fault, symmetrical, and unsymmetrical fault conditions. Section 5 presents the conclusions and recommendations for future work.

METHODS AND SIMULATION

Modelling of the Induction Motor

To analyse the dynamic and transient performance of a three-phase induction motor, a set of nonlinear differential equations derived from fundamental electromagnetic principles is employed. These equations describe the coupled electrical and mechanical dynamics of the machine under both steady-state and transient operating conditions, and are essential for accurately capturing the interaction between the stator and rotor circuits, particularly during disturbances such as faults (Petrushin *et al*., 2019).

The mathematical model is formulated using the direct–quadrature (d–q) axis transformation in a stationary reference frame, which converts the three-phase (abc) system into an equivalent two-axis orthogonal system while preserving the inherent dynamic characteristics of the motor (Vaccarini *et al*., 2017). This transformation significantly simplifies the analysis and facilitates efficient numerical implementation (Sengamalai *et al*., 2022b; Konuhova, 2025).

The model is driven by a balanced three-phase voltage source, with the stator voltage equations initially expressed in the abc variables as in equations (1) – (3) before being transformed into d–q variables. This representation enables effective simulation of the motor's dynamic behaviour in environments such as MATLAB/Simulink, where the nonlinear state equations can be solved to study transient responses and fault conditions.

$$V_{as} = \sqrt{2} \times V_{rms} \times \sin(\omega t) \quad (1)$$

$$V_{bs} = \sqrt{2} \times V_{rms} \times \sin(\omega t - 2\pi/3) \quad (2)$$

$$V_{cs} = \sqrt{2} \times V_{rms} \times \sin(\omega t + 2\pi/3) \quad (3)$$

Where V_{as}, V_{bs}, V_{cs} represent the instantaneous stator phase voltages, while V_m and ω denote the supply voltage amplitude and electrical angular frequency, respectively.

These three-phase voltages are transformed into d-q variables (only two phases) using Park's transformation matrix as shown in equation (4) (Pedra *et al*., 2024).

$$\begin{bmatrix} V_{qs} \\ V_{ds} \\ V_{os} \end{bmatrix} = 2/3 \begin{bmatrix} 1 & -1/2 & -1/2 \\ 0 & -\sqrt{3}/2 & \sqrt{3}/2 \\ 1/2 & 1/2 & 1/2 \end{bmatrix} \begin{bmatrix} V_{as} \\ V_{bs} \\ V_{cs} \end{bmatrix} \quad (4)$$

Hence, the stator circuit equations can be modelled using Figure 1 in a stationary reference frame:

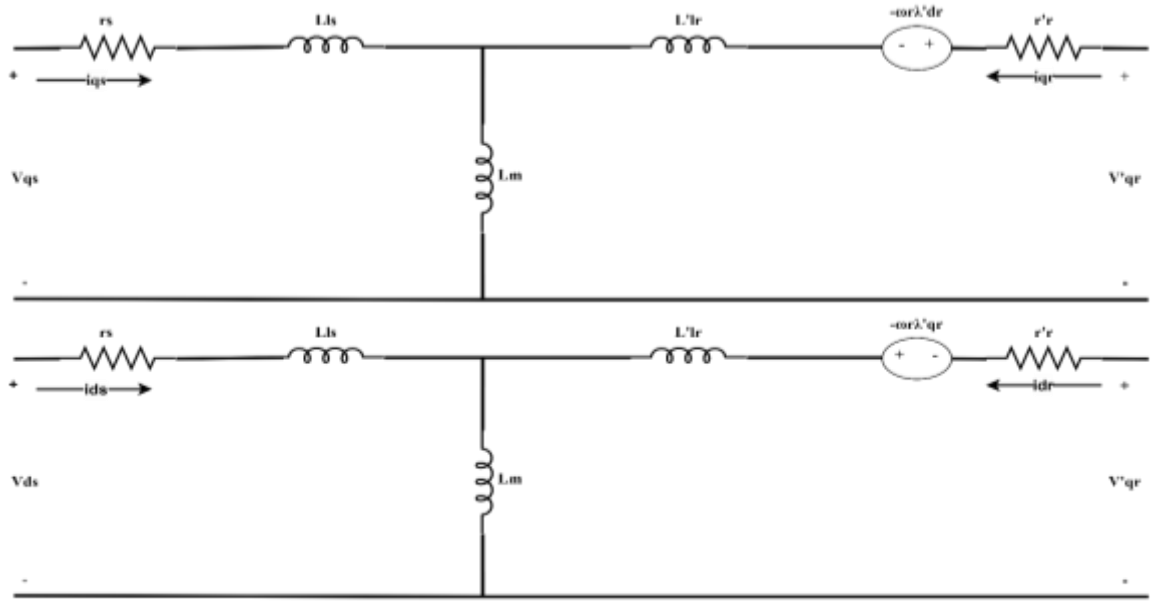


Figure 1: Equivalent circuit of an induction motor in stationary reference frame

$$V_{qs} = r_s i_{qs} + p\lambda_{qs} \quad (5)$$

$$V_{ds} = r_s i_{ds} + p\lambda_{ds} \quad (6)$$

$$V_{os} = r_s i_{os} + p\lambda_{os} \quad (7)$$

$$V`_{qr} = r_r `i_{qr} - \omega_r \lambda`_{dr} + p\lambda`_{qr} \quad (8)$$

$$V`_{dr} = r`_r i`_{dr} + \omega_r \lambda`_{qr} + p\lambda`_{dr} \quad (9)$$

$$V`_{or} = r`_r i`_{dr} + p\lambda`_{or} \quad (10)$$

The flux equations can be expressed in terms of the integral of voltage, current, and resistance from equations (5) - (10) (Kulandaivel *et al*., 2023).

$$\lambda_{qs} = \int V_{qs} - r_s i_{qs} \quad (11)$$

$$\lambda_{ds} = \int V_{ds} - r_s i_{ds} \quad (12)$$

$$\lambda_{os} = \int V_{os} - r_s i_{os} \quad (13)$$

$$\lambda`_{qr} = \int V`_{qr} - r`_r i`_{qr} + \omega_r \lambda`_{dr} \quad (14)$$

$$\lambda`_{dr} = \int V`_{dr} - r`_r i`_{dr} - \omega_r \lambda`_{qr} \quad (15)$$

$$\lambda_{ds} = \int V_{ds} - r_s i_{ds} \quad (16)$$

The torque developed in an Induction machine is modelled in a general form in relation to the q-d axis components of the parameters as in equation (17).

$$T_{em} = \left(3/2\right)\left(p/2\right)\left(\lambda_{ds} i_{qs} - \lambda_{qs} i_{ds}\right) \quad (17)$$

where the λ_{ds}, i_{ds}, λ_{qs} and i_{qs} represent the corresponding d-axis and q-axis flux linkage and current components, while p is the poles pair of the machine.

The mechanical rotor speed equation is expressed as in equation (18);

$$J\,\partial\omega_r/\partial t = T_{em} - T_L \quad (18)$$

Where: J is the rotor inertia, ω_r is the mechanical rotor angular speed, T_{em} is the electromagnetic torque, and T_L is the applied load torque and viscous friction is neglected.

Performance Metrics of Fault Severity

To quantitatively evaluate and compare the dynamic response of the three-phase induction motor under the investigated operating conditions, selected performance metrics were extracted from the simulated stator-current, electromagnetic-torque, and rotor-speed responses. The metrics were evaluated over the defined fault interval, $t_f \le t \le t_c$

where t_f and t_c denote the fault initiation and clearing times, respectively. The pre-fault steady-state values obtained immediately before fault application were used as reference values for determining the magnitude of performance degradation. For the electrical response, the peak stator current I_{peak}, was used to quantify the maximum current surge produced during the fault and is defined as

$$I_{peak} = \max_{t_f \le t \le t_c} |\, i_s(t) \,| \quad (19)$$

Where $i_s(t)$ represents the stator current response. The root-mean-square (RMS) stator current, I_{RMS}, was used to characterise the effective current loading and associated thermal stress on the motor windings during the fault interval and is expressed as

$$I_{RMS} = \sqrt{\frac{1}{t_c - t_f}\int_{t_f}^{t_c} i_s^2(t)\,dt} \quad (20)$$

For the mechanical response, the minimum rotor speed, $N_{\min}$, was determined as the lowest rotor speed attained during the fault interval:

$$N_{\min} = \min_{t_f \le t \le t_c} N_r(t) \quad (21)$$

Where $N_r(t)$ is the rotor speed in revolutions per minute. To provide a normalised measure of speed degradation, the percentage rotor speed reduction, ΔN, was calculated with respect to the pre-fault steady-state speed, N_{pre}, as

$$\Delta N(\%) = \frac{N_{pre} - N_{\min}}{N_{pre}} \times 100 \qquad (22)$$

A larger value of ΔN therefore indicates a greater deterioration in motor speed during the fault. The electromagnetic response was evaluated using the minimum electromagnetic torque, $T_{\min}$, and the peak-to-peak torque variation, ΔT_{pp}. The minimum torque is defined as

$$T_{\min} = \min_{t_f \le t \le t_c} T_e(t) \qquad (23)$$

Where $T_e(t)$ is the electromagnetic torque. The peak-to-peak torque variation, which provides an indication of the magnitude of torque pulsations generated by the fault, is given by

$$\Delta T_{pp} = T_{\max} - T_{\min} \qquad (24)$$

where $T_{\max}$ and $T_{\min}$ are the maximum and minimum electromagnetic torque values within the fault interval, respectively. A larger ΔT_{pp} represents greater torque oscillation and, consequently, a potentially greater mechanical disturbance.

Because line-to-ground, line-to-line, and line-to-line-to-ground faults produce unbalanced phase currents, phase current imbalance was additionally considered for the unsymmetrical fault conditions. The percentage current imbalance was evaluated from the RMS phase currents using

$$I_{imb}(\%) = \frac{I_{\max} - I_{\min}}{I_{avg}} \times 100 \qquad (25)$$

where $I_{\min}$, $I_{\max}$, and I_{avg} are the minimum, maximum, and average RMS values of the three-phase currents, respectively. This metric provides a quantitative indication of the deviation from balanced three-phase operation.

The calculated metrics were subsequently compared across the no-fault, symmetrical-fault, and unsymmetrical-fault conditions. The no-fault case served as the baseline reference, while the faulted cases were evaluated according to their current surge, effective current loading, speed reduction, torque degradation, torque pulsation, and phase-current imbalance. This quantitative approach provides an objective basis for assessing the relative severity and dynamic characteristics of the investigated faults and complements the time-domain waveform analysis presented in the Results and Discussion section.

MATLAB/Simulink IMPLEMENTATION

The dynamic model of the induction motor, formulated in the d-q reference frame, is implemented in MATLAB/Simulink to investigate its transient and steady-state performance under no-load conditions. The mathematical model, as presented in the equations above, was implemented. Figure 2 illustrates the complete Simulink model of the three-phase induction motor. The model was simulated from standstill. The complete simulation duration was 3 s, and a variable step solver (ode23tb) with relative and absolute tolerances of 10^{-4} and 10^{-6}, respectively. The same motor parameters and simulation settings were retained for all operating scenarios to ensure that differences in the responses were attributable primarily to the applied fault condition.

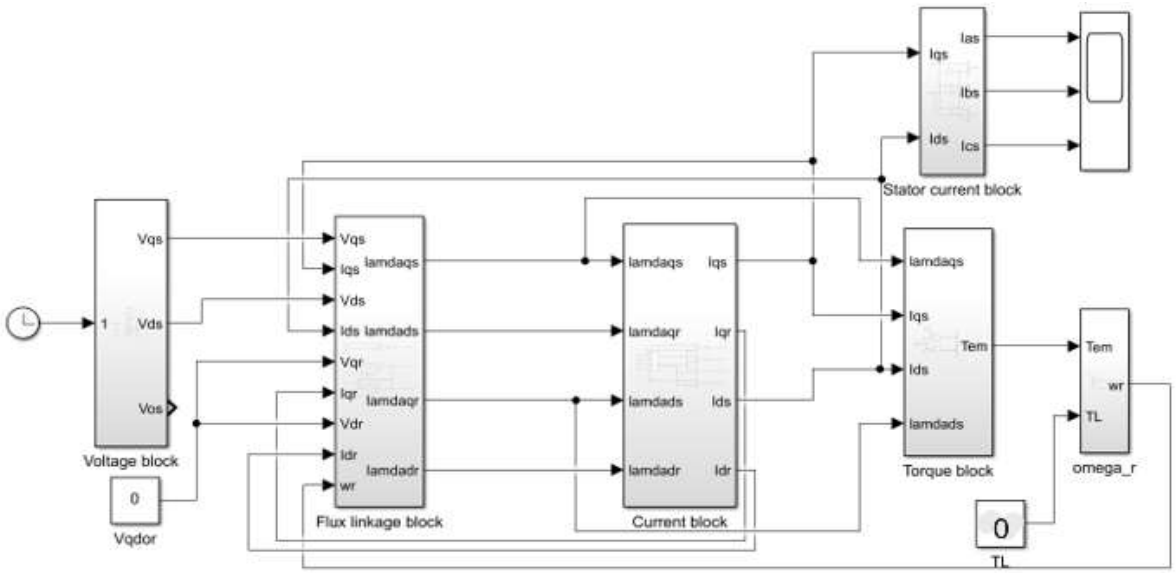


Figure 2: Overview of the complete dynamic model in MATLAB/Simulink

The simulation was carried out on a 3 hp, 60 Hz, 4-pole, 220 V star-connected induction motor. The motor specifications used in the simulations are summarised in Table 1.

Table 1: Induction machine specifications

Parameters	Ratings
Rated power	3 hp (2.24 kW)
Rated voltage	220 V
Frequency	60 Hz
Number of poles	4
Connection	Star
Stator resistance (Rs)	0.435 Ω
Rotor resistance (Rr)	0.816 Ω
Magnetising inductance (Lm)	0.0693 H
Rotor leakage inductance (Llr)	0.001999 H
Stator leakage inductance (Lls)	0.001999 H
Rotor self-inductance	Llr + Lm
Stator self-inductance	Lls + Lm
Inertia (J)	0.089 kgm^2

Fault Scenario Simulation

The fault conditions were implemented at the motor terminals using controlled switching elements in MATLAB/Simulink. Five operating scenarios were considered: no-fault, three-phase fault (A – B – C), L–G fault (A – G), L–L fault (B – C), and L–L–G fault (B – C – G). The same source voltage, frequency, motor parameters, initial conditions, simulation settings, and fault impedance assumed to be negligible were maintained for all cases to ensure a consistent comparative basis. The fault initiation time is at 1.5 s, the fault duration is 0.5 s, giving a clearing time of 2.0 s. Consequently, the simulation was divided into three operating intervals $0 \le t \le 1.5s$ representing the pre-fault interval while, $1.5 \le t \le 2.0s$ represents the fault interval, and $2.0 \le t \le 3.0s$ represents the post-fault recovery interval.

This arrangement allows the motor response to be evaluated prior to fault initiation, during the electrical fault, and following fault clearance. The fault duration was kept constant for all fault types so that the comparative analysis was not influenced by differences in fault duration. The fault responses were recorded in terms of stator currents, electromagnetic torque, and rotor speed. The quantitative metrics defined in Section 2.3 were subsequently extracted from the corresponding simulation data. The no-fault response provided the baseline operating condition, while the fault cases were compared with their peak current, RMS current, speed degradation, torque response, torque pulsation, and phase-current imbalance.

RESULTS AND DISCUSSION

The findings are presented in five subsections: no-fault condition, symmetrical fault condition, and unsymmetrical fault condition. The waveforms illustrate the transient and dynamic response of an induction motor.

Baseline No-fault Condition

The dynamic response of the no-fault simulation is shown in Fig. 3; this is set as the baseline condition for evaluating other fault scenario responses. Fig. 3b shows that the electromagnetic torque has a large startup transient, approximately 196.13 Nm, then reduces as the rotor accelerates and the slip is reduced. The electromagnetic torque was close to steady-state after the acceleration transient. As the torque reduces, the rotor speed increases close to the synchronous speed; this is physically related to a reduction in slip and the induced current by the rotor. The torque settled around 0.2 s, which shows that the motor had reached its normal electromechanical operating state before the fault was initiated at 1.5 s.

The rotor accelerated toward the synchronous speed of 1800 rpm from standstill, presenting typical dynamics of a 4-pole, 60-Hz supply used in the simulation. The motor rotor settled at a steady-state speed of approximately 1800 rpm, as shown in Figure 3c, showing that a small slip is required for torque production in an induction motor and that the speed response remained stable, with no noticeable oscillation behaviour after the startup acceleration period. This response is consistent with the dynamic behaviour of an induction motor, agreeing with existing mathematical and simulation-based investigations (Konuhova, 2025; Zhou *et al*., 2024).

Figure 3d illustrates the stator current, which exhibited transients associated with motor startup and a reduced rotor acceleration and increased back electromotive force. Table 2 shows that for no-fault, the peak current is 11.58 A and the RMS current is 8.19 A. These values serve as the reference for assessing the current disturbances caused by the fault conditions.

Generally, the no-fault response established that the implemented d-q model replicates the main dynamic characteristics expected from an induction motor. The reference is therefore suitable for assessing the deviation caused by the different fault conditions.

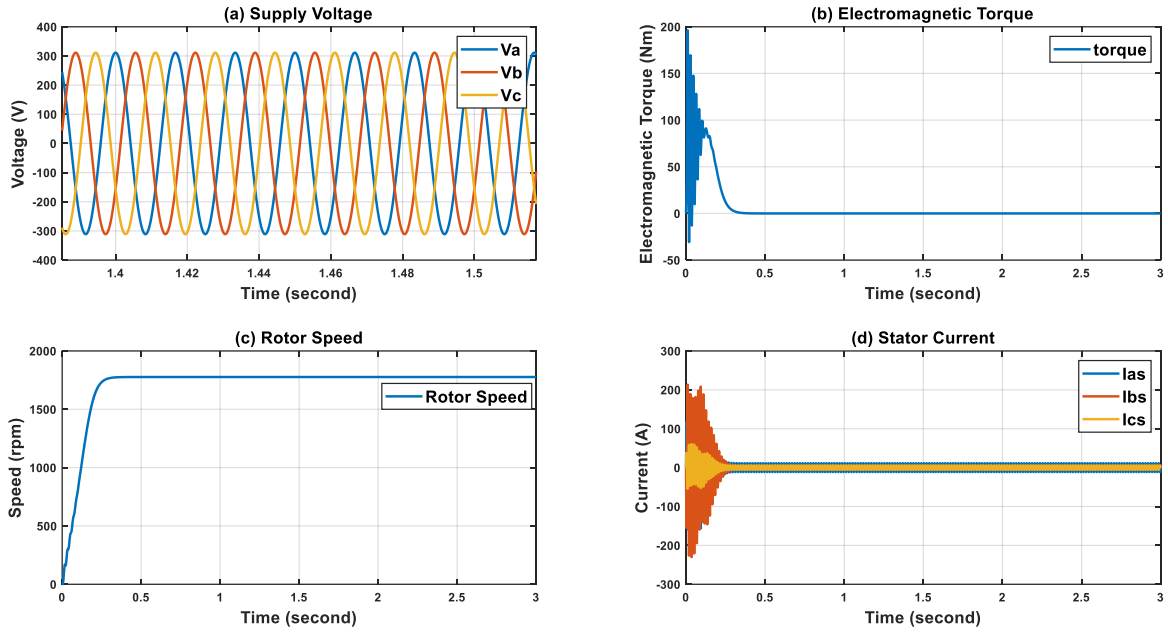


Figure 3: (a) Supply voltage at no-fault, (b) Electromagnetic torque at no-fault, (c) Rotor speed at no-fault, (d) Stator current at no-fault

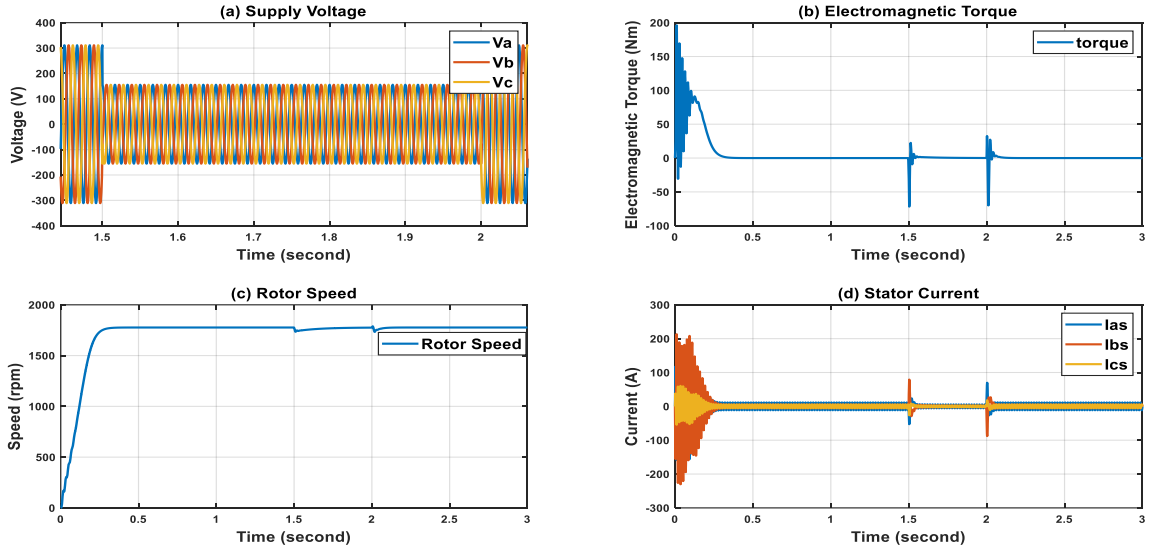


Figure 4: (a) Supply voltage at symmetrical fault, (b) Electromagnetic torque at symmetrical fault, (c) Rotor speed at symmetrical fault, (d) Stator current at symmetrical fault

Dynamic Response under Three-phase Symmetrical Fault

Figure 4a shows the three-phase symmetrical fault case, represented by the three phases of the motor supply being subjected to the same fault condition. Figure 4b shows that the electromagnetic torque undergoes a more noticeable disturbance. The torque dips sharply and oscillates through the negative region immediately after the fault was introduced. The minimum electromagnetic torque reaches −71.71 Nm, while the peak-to-peak torque variation is 94.18 Nm. The negative torque represents a temporary reversal of the electromagnetic torque component relative to the normal motoring direction. This response shows disruption of the electromagnetic energy conversion process during the fault. This shows the importance of electromagnetic torque.

Figure 4c shows that the motor follows the regular pre-fault trajectory until the fault is initiated at 1.5 s. The minimum rotor speed observed was 1734.14 rpm, which is a 2.39% reduction in speed from the pre-fault rotor speed. This small speed deviation shows that the mechanical characteristics of the motor are not severely affected by the fault. But the effect of the fault is noticed in the transient speed response. This study shows that a fault can cause severe disturbance in electrical and electromagnetic characteristics of an induction motor without necessarily causing a significant reduction in rotor speed.

Figure 4d shows the electrical response, the stator current increases sharply after fault initiation. The peak current increases from the no-fault value of 11.58 A to 79.08 A, and the RMS current increases to 9.10 A. Hence, the variation in the peak current is more noticeable than the change in RMS current, which means that the fault produces a high instantaneous current deviation but a small increase in the effective current over the evaluated interval.

The three-phase fault shows a 47.81% current imbalance. This is not a confirmation that the fault is inherently unsymmetrical because theoretically a three-phase fault is symmetrical. This should be interpreted together with the phase current waveforms and not as a steady-state imbalance index. This is important because this study mainly aims at using the current imbalance as a peculiar characteristic for unsymmetrical fault cases.

In summary, the three-phase fault causes a large instantaneous current surge, torque collapse, and a very small reduction in rotor speed. Hence, its effect is more evident in the electrical and electromagnetic responses than in the minimum rotor speed metric. This result points to the importance of various performance indicators to identify the severity of faults in induction motors.

Dynamic Response under Single Line-to-ground (L-G) Fault

The dynamic response of the induction motor is shown in Fig. 5 exhibit a characteristic which aggress with previous studies on induction motor faults (Hussain, 2021; Maraaba *et al*., 2018) that asymmetric stator conditions can result in unbalanced phase current and characteristic changes in electromagnetic and mechanical variables. A L–G fault is simulated, and the waveform is illustrated in Fig. 5a, which shows the unbalanced electrical disturbance because one phase is directly involved in the fault.

The electromagnetic torque reduces abruptly and exhibits oscillating behaviour that extends into the negative region at fault initiation, as shown in Fig. 5b. The minimum torque is −32.93 Nm, while the peak-to-peak torque variation reaches 68.07 Nm. These oscillations show that the asymmetric electrical fault changes the electromagnetic energy conversion process even though the rotor speed deviation remains comparatively small.

Figure 5c shows the rotor speed behaviour; this follows the baseline trajectory before the fault is introduced at 1.5 s. A reduction of 0.70% in rotor speed to 1764.10 rpm is recorded; this is the minimum speed reduction in all fault case scenarios. This small variation in rotor speed suggests that the overall effect of the L–G fault is relatively small. This indicates that the L–G fault produces a comparatively insignificant disturbance to the overall rotational motion during the specified fault interval. The small speed reduction, however, does not imply that the L–G fault is electrically insignificant.

Figure 5d shows the current response. The peak stator current increases to 91.32 A compared to 79.08 A, and the RMS current increases to 57.32 A compared to 9.10 A obtained for the three-phase fault. The phase current imbalance is 60.39% although the L–G fault produces the smallest percentage rotor speed reduction; it produces a considerably larger effective current loading and greater phase asymmetry than the three-phase fault.

This result has significant relevance for evaluating faults. If rotor speed reduction were used exclusively as an indicator, the L–G fault would be identified as the least important fault. However, the RMS current and current imbalance results show that the fault places a significant electrical stress on the motor. This agrees with the general finding in induction motor condition monitoring those different measurable signals can exhibit different sensitivities to a particular fault, this makes it important to use multiple complementary indicators (Gangsar & Tiwari, 2020; Hamani *et al*., 2025).

The L–G case clearly demonstrated why fault severity should not be deduced from rotor speed alone. The primary characteristic signature in this simulation is a combination of relatively small mechanical speed reduction, current loading, phase current imbalance, and electromagnetic torque oscillation.

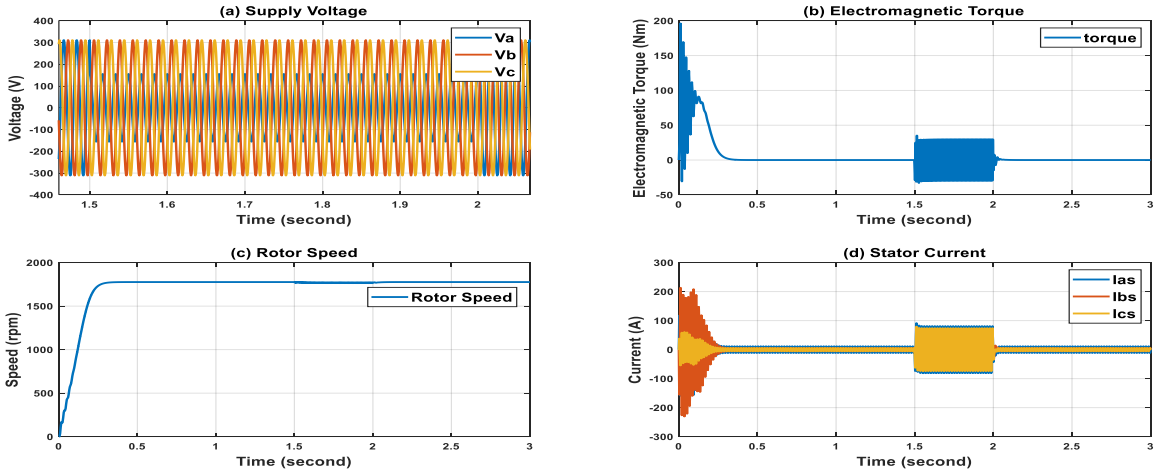


Figure 5: (a) Supply voltage at an unsymmetrical (L-G) fault, (b) Electromagnetic torque at an unsymmetrical (L-G) fault, (c) Rotor speed at an unsymmetrical (L-G) fault, (d) Stator current at an unsymmetrical (L-G) fault

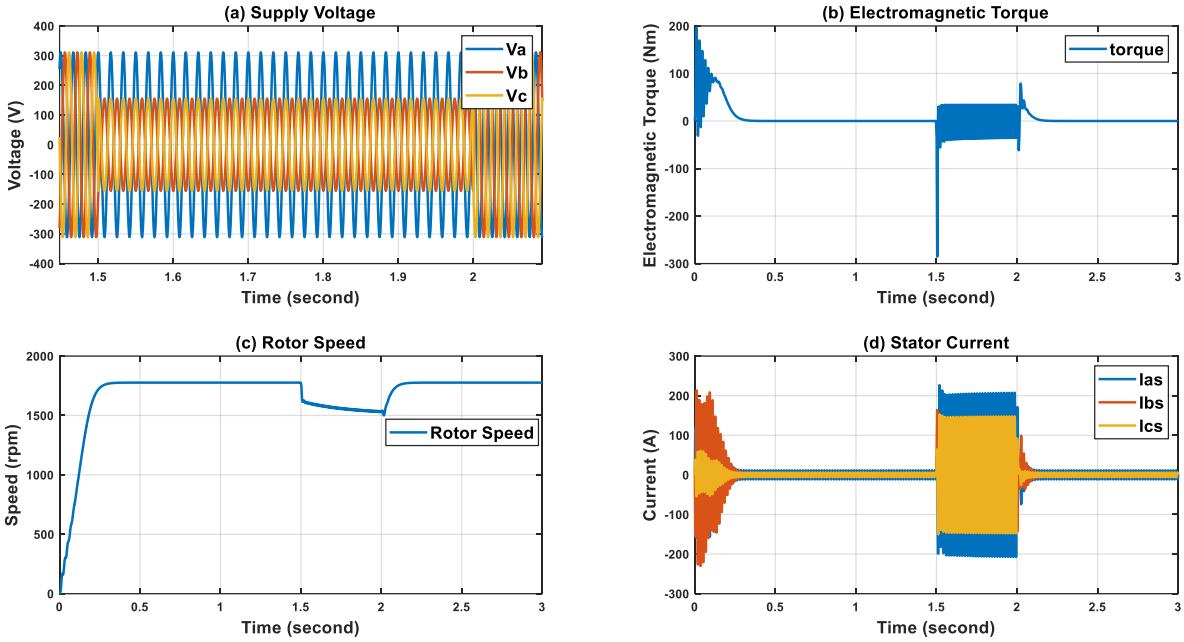


Figure 6: (a) Supply voltage at unsymmetrical (L-L) fault, (b) Electromagnetic torque at unsymmetrical (L-L) fault, (c) Rotor speed at unsymmetrical (L-L) fault, (d) Stator current at unsymmetrical (L-L) fault

Dynamic Response under Line-to-line (L-L) Fault

Figure 6 presents the dynamic response under L–L fault, it produces the most severe disturbance when peak current, RMS current, rotor speed reduction, minimum torque, and torque peak-to-peak variation are considered. Figure 6b shows the mechanical response, which is accompanied by a large electromagnetic torque oscillation. The minimum torque of −285.23 Nm was observed, while the peak-to-peak torque variation is 319.49 Nm, both representing the highest values among the fault cases. The magnitude of this torque deviation shows a severe disturbance of the electromagnetic energy conversion process. The negative torque also complements the reduced rotor speed observed during the fault.

At 1.5 s, when the fault was introduced as in Fig. 6c, the rotor speed decreases rapidly, deviating from its pre-fault steady-state speed to about 1527.26 rpm, a 14.03% reduction in speed. This is the highest speed deviation in all the investigated fault conditions.

The electrical response is similarly severe. Fig. 6d shows the stator current, the peak stator current is 226.62 A, compared with the no-fault condition, with peak current of 11.58 A. The RMS current is 144.04 A, while the phase current imbalance is 46.05%. The peak current is roughly 19.6 times the reported no-fault condition peak-current value. The high current deviation indicates significant electrical stress during the L–L fault.

It is important to note that the L–L fault does not produce the highest phase current imbalance. Its 46.05% imbalance is lower than the 60.39% obtained for the L–G fault and the 70.69% obtained for the L–L–G fault. However, it produces considerably larger peak and RMS current, speed reduction, and torque deviation. This proves that phase asymmetry and overall fault severity are not the same. The L–L fault is therefore best characterised by its high current magnitude, severe mechanical speed reduction, and very large electromagnetic torque deviation.

This result agrees with the general principle that electrical faults affect the coupled electrical and mechanical subsystems of an induction motor rather than a single measurable variable. Fault modelling research also highlights the need to consider multiple machine variables when evaluating the dynamic impact of abnormal conditions (Terron-Santiago *et al*., 2021).

Dynamic Response under Double Line-to-ground (L-L-G) Fault

The L–L–G fault presents a severe asymmetric fault due to the simultaneous involvement of two phases with the ground, as shown in Fig. 7a. The electromagnetic torque response demonstrates significant oscillation characteristics after the fault was introduced, as shown in Fig. 7b. The minimum torque is −184.66 Nm, while the peak-to-peak torque variation is 204.13 Nm. Though the minimum torque magnitude is less than that of the L–L fault, the torque deviation remains much greater than that of the three-phase and L–G faults. This shows that the L–L–G fault produces a significant disturbance in electromagnetic energy conversion and contributes significantly to the reduction in rotor speed.

Figure 7c shows the rotor speed response; the motor follows the normal pre-fault trajectory until the fault is initiated at 1.5 s, after which the rotor speed decreases to 1566.84 rpm, which causes a 11.80% speed reduction, which is greater than those obtained for the three-phase and L–G faults but lower than the 14.03% obtained for the L–L fault.

The electrical response in Fig. 7d further establishes the severity of the L–L–G condition. The peak stator current and RMS current are 210.93 A and 133.57 A,

respectively. A corresponding phase current imbalance of 70.69%, which is the highest imbalance among all the investigated fault cases. The combination of high RMS current and current asymmetry makes the L–L–G fault more critical regarding electrical loading and phase imbalance.

The L–L–G case holds a significant position in the comparative analysis. Though its peak current and torque deviation are less than those of the L–L fault, it produces the highest phase current imbalance and the second highest RMS current. The result establishes that a fault involving two phases and ground can impose significant electrical and electromechanical stress even when another fault type produces a higher instantaneous current peak.

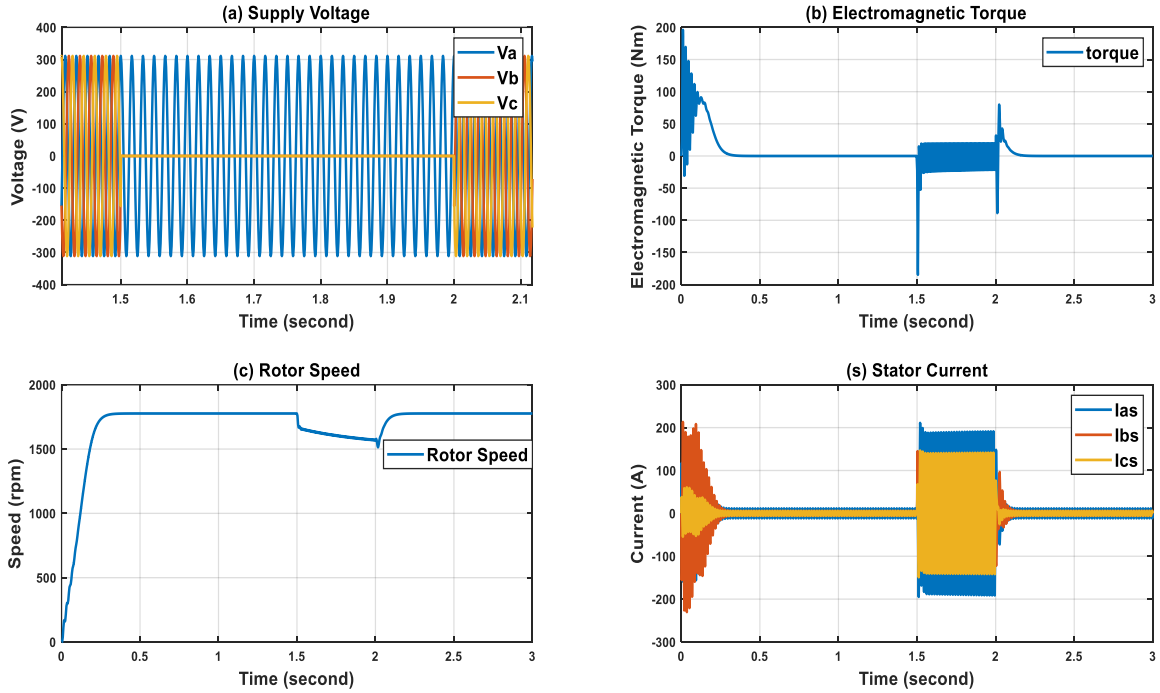


Figure 7: (a) Supply voltage at unsymmetrical (L-L-G) fault, (b) Electromagnetic torque at unsymmetrical (L-L-G) fault, (c) Rotor speed at unsymmetrical (L-L-G) fault, (d) Stator current at unsymmetrical (L-L-G) fault

Table 2: Fault-severity analysis

Fault condition	I_{peak} (A)	I_{RMS} (A)	N_{min} (rpm)	Speed reduction (%)	T_{min} (Nm)	$Torque_{(p-p)}$ (Nm)	Current imbalance (%)
No fault	11.58	8.19	1776.53	-	0	-	-
Three-phase fault	79.08	9.10	1734.14	2.39	-71.71	94.18	47.81
L-G fault	91.32	57.32	1764.10	0.70	-32.93	68.07	60.39
L-L fault	226.62	144.04	1527.26	14.03	-285.23	319.49	46.05
L-L-G fault	210.93	133.57	1566.84	11.80	-184.66	204.13	70.69

Comparative Fault-severity Analysis

Table 2 presents the quantitative comparison of the simulated conditions. The results establish that the effects of the different faults cannot be effectively characterised by a single severity ranking, as each fault produces a different combination of electrical, mechanical, and electromechanical disturbances.

The no-fault condition creates the benchmark motor response, with a peak current and RMS current of 11.58 A and 8.19 A, respectively, and a steady-state rotor speed of 1776.53 rpm. The fault scenarios show greater disturbances in all the three dynamic response variables. The three-phase fault resulted in an increase in peak current to 79.08 A and reduced the minimum rotor speed to 1734.14 rpm, which is about a 2.39% reduction with reference to the no-fault condition. The minimum electromagnetic torque also decreases to −71.71 Nm.

The L–G fault has the least rotor speed reduction among all the fault scenarios, with a minimum speed of about 1764.10 rpm. However, its RMS current increases to 57.32 A, and its electromagnetic torque is −32.93 Nm. Thus, the speed deviation is relatively small, but this does not imply that the fault is electrically insignificant. The 60.39% current imbalance further confirms the asymmetric nature of the disturbance.

The L–L fault has the highest peak current, reaching 226.62 A, and the largest torque peak-to-peak variation, reaching 319.49 Nm. It also has the minimum rotor speed

of 1527.26 rpm, indicating transient rotor speed. These results identify the L–L fault as the most severe case with respect to instantaneous current surge and torque deviation.

The peak current of the L–L–G fault is significantly lower than that of the L–L fault, 210.93 A versus 226.62 A, and the RMS current is 133.57 A while the maximum current is 70.69%. It also gives a minimum rotor speed of about 1566.84 rpm. These results show that the L–L–G fault is critical in terms of sustained current loading, phase asymmetry, and mechanical speed disturbance.

The results therefore establish that the investigated faults cannot be placed reliably on a single linear severity scale. Instead, their severity depends on the response variable utilised for assessment. This is a key difference when compared to the conventional waveform-based comparison, where the fault producing the visually highest current or torque response might simply be selected as the most severe. The quantitative results show that the L–L fault leads the peak current and torque disturbance, whereas the L–L–G fault leads phase-current imbalance. The L–G fault produces the least rotor speed deviation but still imposes large electrical stress.

Fault Response Interpretation

The combined results show that the fault type determines how the electrical disturbance is transferred into the mechanical and electromagnetic states of the induction motor. The three-phase fault produces a relatively uniform disturbance across the phases and is characterised in this simulation by a strong current surge and torque collapse but comparatively limited rotor speed degradation. The unsymmetrical faults introduce additional phase dependent effects, resulting in unequal phase currents and stronger current imbalance signatures. Such phase dependent behaviour is consistent with the role of asymmetrical electrical conditions in induction motor fault diagnosis and condition monitoring (Hamani *et al*., 2025; Maraaba *et al*., 2018).

The L–G result is useful because it shows that the mechanical response alone can underestimate the severity of an electrical fault. Moreover, it has the minimum percentage speed reduction of 0.70%, but its RMS current is 57.32 A, and its phase current imbalance is 60.39%. Hence, a condition monitoring system or technique exclusively depending on rotor speed response could therefore fail to sufficiently represent the electrical effects of this fault.

Conversely, in all the fault scenarios, the L–L fault causes the most severe disturbance in the measured electrical, mechanical, and electromagnetic responses, except for phase current imbalance. It has a peak current and RMS current of 226.62 A and 144.04 A respectively, which shows severe electrical loading, while the speed reduction of 14.03% and 319.49 Nm torque deviation reflect the corresponding electromechanical effects. The result shows the strong coupling between the electrical fault and the mechanical dynamics represented by the induction motor model (Konuhova, 2025; Zhou *et al*., 2024).

The L–L–G fault presents another essential but different signature. The peak current is a little lower than that of the L–L fault, but the RMS current remains very high, and its phase current imbalance is 70.69%, the highest value recorded. This shows that the L–L–G fault is very important when the objective of the condition monitoring technique is to detect phase asymmetry and continuous electrical loading, rather than the highest instantaneous current.

Fault severity should be viewed as a multidimensional rather than a single ordered parameter, which is an important conclusion of these findings. Minimum torque and peak-to-peak torque quantify electromagnetic disruption; rotor speed reduction reflects the mechanical effect of the disturbance; phase current imbalance captures the asymmetrical nature of the unsymmetrical faults; peak current is primarily sensitive to instantaneous electrical stress; and RMS current provides information on effective electrical loading. The use of complementary indications is in line with the larger body of literature on condition monitoring, which highlights the need to extract multiple diagnostic features from induction motor responses rather than depending on one signal (Gangsar & Tiwari, 2020; Hamani *et al*., 2025).

The results also demonstrate a meaningful comparison with the closely related MATLAB/Simulink study by (Sebastian *et al*., 2024), which showed that under symmetrical and unsymmetrical faults, rotor speed, electromagnetic torque, and stator current exhibit clear changes. By quantitatively extracting several electrical, mechanical, and electromechanical indications from the same simulation framework, the current study expands on this kind of waveform-based analysis. This offers a clearer foundation for comparing the unique signatures of the different fault conditions.

Overall, the findings show that no single measured variable is adequate for complete fault characterisation. Rotor speed and electromagnetic torque show the mechanical and electromechanical effects of the disturbance, whereas electrical variables reveal current stress and phase asymmetry. Thus, the combined metric framework can be used as a basis for future model-based protection, condition monitoring, and automated fault classification studies. It also offers a more objective basis for differentiating the fault conditions under investigation.

CONCLUSION

This study investigated the dynamic behaviour of a three-phase induction motor under no-fault, symmetrical, and unsymmetrical electrical fault conditions using a stationary reference frame d-q mathematical model implemented in MATLAB/Simulink. Five operating conditions were considered: no-fault operation, three-phase fault, line-to-ground (L–G) fault, line-to-line (L–L) fault, and double line-to-ground (L–L–G) fault. The faults were introduced at the motor terminal at 1.5 s and cleared after 0.5 s within a total simulation period of 3 s. The analysis combined stator current, electromagnetic torque, and rotor speed responses with quantitative fault

signature metrics to provide an objective comparison of the investigated conditions.

A key outcome established a multidimensional fault signature assessment. Peak current provides information about instantaneous electrical stress, RMS current indicates effective current loading, rotor speed reduction quantifies mechanical degradation, torque-related metrics characterise electromagnetic disturbance, and phase current imbalance provides an indication of asymmetry. The combined use of these metrics provides a more comprehensive basis for distinguishing the investigated fault conditions than qualitative inspection of individual waveforms alone.

The developed simulation framework provides a useful foundation for induction motor fault characterisation, condition monitoring, and subsequent model based diagnostic development. However, the present investigation is simulation based and considers a defined set of fault types and operating conditions. Future work should therefore extend the analysis to experimental validation, different fault impedances and fault locations, varying load conditions, parameter uncertainties, and automated fault classification using statistical or machine-learning techniques. Such extensions would further establish the applicability of the proposed quantitative fault signature framework to practical induction motor protection and condition monitoring systems.

Conflict of interest: The authors declare no conflict of interest.

REFERENCES

Al hajzber, S. M., Ali, A. J., AL-Rifaie, A. H. and Shanshal, A. K. (2021). A comparative study for the performance operation of electric machine based on conventional and D-Q theories. *Int. Journal of Power Electronics and Drive Systems (IJPEDS)*, 12(3), 1304. https://doi.org/10.11591/ijpeds.v12.i3.pp1304-1314

Bahgat, B. H., Elhay, E. A. and Elkholy, M. M. (2024). Advanced fault detection technique of three phase induction motor: comprehensive review. *Discover Electronics*, 1(1), 9. https://doi.org/10.1007/s44291-024-00012-3

Dawood, A., Hasaneen, B. M. and Abdel-Aziz, A. M. (2024). Design of an efficient neural network model for detection and classification of phase loss faults for three-phase induction motor. *Neural Computing and Applic.*, 36(11), 5827–5845. https://doi.org/10.1007/s00521-023-09387-y

Gangsar, P. and Tiwari, R. (2020). Signal based condition monitoring techniques for fault detection and diagnosis of induction motors: A state-of-the-art review. *Mechanical Systems and Signal Processing*, 144, 106908. https://doi.org/10.1016/j.ymssp.2020.106908

Hamani, K., Kuchar, M., Kubatko, M. and Kirschner, S. (2025). Advancements in Induction Motor Fault Diagnosis and Condition Monitoring: A Comprehensive Review. *Sensors*, *25*(19), 5942. https://doi.org/10.3390/s25195942

Hussain, M. (2021). Stator Winding Fault Detection and Classification in Three-Phase Induction Motor. *Intelligent Automation & Soft Comp.*, 29(3), 869–883. https://doi.org/10.32604/iasc.2021.017790

Reyes-Malanche, J. A., Ramirez-Velasco, E., Villalobos-Pina, F. J. and Gadi, S. K. (2024). Short-Circuit Fault Diagnosis on the Windings of Three-Phase Induction Motors through Phasor Analysis and Fuzzy Logic. *Energies*, 17(16), 4197. https://doi.org/10.3390/en17164197

Sapena-Bano, A., Chinesta, F., Puche-Panadero, R., Martinez-Roman, J. and Pineda-Sanchez, M. (2021). Model reduction based on sparse identification techniques for induction machines: Towards the real time and accuracy-guaranteed simulation of faulty induction machines. *International Journal of Electrical Power & Energy Systems*, 125, 106417. https://doi.org/10.1016/j.ijepes.2020.106417

Sebastian, E. U., Okpo, E. E. and Nkan, I. E. (2024). Dynamic Simulation and Analysis of Three Phase Induction Motor for Faults Detection using Matlab/Simulink. *Journal of Engineering Research and Reports*, 26(11), 286–303. https://doi.org/10.9734/jerr/2024/v26i111331

Sengamalai, U., Anbazhagan, G., Thamizh Thentral, T. M., Vishnuram, P., Khurshaid, T. and Kamel, S. (2022a). Three Phase Induction Motor Drive: A Systematic Review on Dynamic Modeling, Parameter Estimation, and Control Schemes. *Energies*, 15(21), 8260. https://doi.org/10.3390/en15218260

Sengamalai, U., Anbazhagan, G., Thamizh Thentral, T. M., Vishnuram, P., Khurshaid, T. and Kamel, S. (2022b). Three Phase Induction Motor Drive: A Systematic Review on Dynamic Modeling, Parameter Estimation, and Control Schemes. *Energies*, 15(21), 8260. https://doi.org/10.3390/en15218260

Terron-Santiago, C., Martinez-Roman, J., Puche-Panadero, R. and Sapena-Bano, A. (2021). A Review of Techniques Used for Induction Machine Fault Modelling. *Sensors*, 21(14), 4855. https://doi.org/10.3390/s21144855

Vaccarini, M., Carbonari, A. and Casals, M. (2017). Development and calibration of a model for the dynamic simulation of fans with induction motors. *Applied Thermal Engr.*, 111, 647–659. https://doi.org/10.1016/j.applthermaleng.2016.09.080

Zhou, Z., Chen, Z. and Zhai, W. (2024). Dynamics modeling and electromechanical coupling characteristics analysis of cage induction motors. *Science China Technological Sci.*, 67(3), 709–724. https://doi.org/10.1007/s11431-023-2561-2